

TESTING EUV/X-RAY ATOMIC DATA FOR THE *SOLAR DYNAMICS OBSERVATORY*PAOLA TESTA¹, JEREMY J. DRAKE¹, ENRICO LANDI²*Draft version October 21, 2011*

ABSTRACT

The Atmospheric Imaging Assembly (AIA) and the Extreme-ultraviolet Variability Experiment (EVE) onboard the Solar Dynamics Observatory include spectral windows in the X-ray/EUV band. Accuracy and completeness of the atomic data in this wavelength range is essential for interpretation of the spectrum and irradiance of the solar corona, and of SDO observations made with the AIA and EVE instruments. Here we test the X-ray/EUV data in the CHIANTI database to assess their completeness and accuracy in the *SDO* bands, with particular focus on the 94Å and 131Å AIA passbands. Given the paucity of solar observations adequate for this purpose, we use high-resolution X-ray spectra of the low-activity solar-like corona of Procyon obtained with the *Chandra* Low Energy Transmission Grating Spectrometer (LETGS). We find that while spectral models overall can reproduce quite well the observed spectra in the soft X-ray range $\lambda \lesssim 50\text{Å}$, and at the EUV wavelengths $\lambda \gtrsim 130\text{Å}$, they significantly underestimate the observed flux in the 50-130Å wavelength range. The model underestimates the observed flux by a variable factor ranging from ≈ 1.5 , at short wavelengths below $\sim 50\text{Å}$, up to $\approx 5\text{--}7$ in the $\sim 70\text{--}125\text{Å}$ range. In the AIA bands covered by LETGS, i.e. 94Å and 131Å, we find that the observed flux can be underestimated by large factors (~ 3 and ~ 1.9 respectively, for the case of Procyon presented here). We discuss the consequences for analysis of AIA data and possible empirical corrections to the AIA responses to model more realistically the coronal emission in these passbands.

Subject headings: Sun: corona, Sun: X-rays, Stars: late-type, Stars: individual: Procyon, Stars: coronae, X-rays: stars

1. INTRODUCTION

The solar EUV and X-ray radiation plays a double role in the physics of the solar upper atmosphere: by representing an important term in the energy equation, and by bearing the signatures of the most important physical phenomena that occur during solar activity, namely, flares and coronal mass ejections (CMEs). It is also one of the primary energy inputs to the Earth's upper atmosphere: it heats the thermosphere, creates the ionosphere, and drives a number of dynamical motions and photochemical reactions at different heights. By its own nature, the EUV and X-ray emission of the Sun is highly variable on all time scales, from a factor two to several orders of magnitude (Woods et al. 2004). The largest variations occur at the shortest wavelengths.

The 10-170 Å region includes a large number of spectral lines emitted by highly ionized species formed at temperatures at, or above, 1 MK. These lines dominate the EUV solar irradiance, and are of crucial importance for investigating the interaction between the solar radiative output and the Earth's upper atmosphere. For example, Pawlowski & Ridley (2008) showed that flare radiation, dominated by highly ionized Fe transitions in the 90-140 Å range, can increase the density of the Earth's thermosphere by as much as $\approx 15\%$ in less than two hours. These lines also provide excellent diagnostic tools for measuring the physical properties of the emit-

ting plasmas under quiescent, active and flaring conditions. Furthermore, key ions routinely detected by *in-situ* measurements of the solar wind (O VII, VIII, C V, VI) emit very strong lines between 18 Å and 40 Å.

In recent years, the 10-170 Å range has attracted considerable attention because of several instruments, both already launched and being developed, that can observe astrophysical objects in this spectral interval. *EUVE*, *Chandra* and *XMM-Newton* obtained high-resolution spectra from all kinds of astrophysical objects, while the Thermosphere Ionosphere Mesosphere Energetics and Dynamics and Solar EUV Experiment (TIMED/SEE) and the recently launched Solar Dynamic Observatory (*SDO*) include instrumentation aimed at studying the solar corona, the solar irradiance and their variability using this range. In particular, the Extreme Ultraviolet Variability Experiment (EVE, Woods et al. 2010) and the Atmospheric Imaging Assembly (AIA, Lemen et al. 2011; Boerner et al. 2011) on board *SDO* include spectral windows in the 10-170 Å range aimed at studying the energy input, storage and release mechanisms that rule coronal heating and the variability of the solar spectrum. AIA is a suite of 4 telescopes providing high cadence (~ 12 s, for the standard observing mode, though higher cadence is possible) full Sun observations in 7 EUV narrow passbands, at high spatial resolution ($\sim 0.6''/\text{pixel}$): six EUV narrowbands are centered around 94Å, 131Å, 171Å, 195Å, 211Å, 335Å, respectively, which are generally dominated by emission of plasma at temperatures $\log(T[K]) \gtrsim 5.7$. AIA also observes cooler plasma in the 304Å channel (dominated by He II emission) and in a UV channel (where three passbands can be selected at λ

¹ Smithsonian Astrophysical Observatory, 60 Garden street, MS 58, Cambridge, MA 02138, USA; ptesta@cfa.harvard.edu

² Department of Atmospheric, Oceanic and Space Sciences, University of Michigan 2455 Hayward St., Ann Arbor MI 48109 USA

1600Å, 1700Å, 4500Å). EVE measures the full disk solar irradiance in the EUV and soft X-ray energy range (from 1 to 1050Å), with a cadence of 10s. EVE spectral resolution is $\sim 1\text{\AA}$ between 50 and 1050Å (with the *Multiple EUV Grating Spectrographs* MEGS-A and MEGS-B), and 10Å in the 1-50Å range (with MEGS-SAM). EVE also includes an EUV Spectrophotometer (ESP) measuring the irradiance in broad bands in the 1-390Å range, and a MEGS-Photometer (MEGS-P) measuring the hydrogen Lyman- α line at 1216Å.

In order to understand the solar EUV and X-ray spectrum, as well as using it for diagnostic purposes, theoretical models of the sources in the solar atmosphere need to be combined with spectral models (such as CHIANTI - Dere et al. 1997, 2009 - and APEC - Smith et al. 2001; Foster et al. 2010) that can compute it. A key issue in such modeling is the accuracy and completeness of the spectral models: inaccurate or incomplete sets of atomic data and transition rates can jeopardize the success of any modeling effort. Also, the narrow-band filters in the AIA instrument can be used for quantitative scientific purposes only if the spectrum in the wavelength range they cover is known with accuracy. For this reason, available spectral models need to be benchmarked with observations. Benchmarking spectral codes by comparison with X-ray (1-20 Å, Phillips et al. 1999; Landi & Phillips 2006), EUV (170-630 Å, Young et al. 1998; Landi et al. 2002a) and UV (500-1600 Å, Landi et al. 2002b) high-resolution spectra revealed some discrepancies and led to substantial improvements in the available data. Benchmark studies focusing on the 20-170 Å range are limited, such as, for instance, the work by Del Zanna & Ishikawa (2009) who carried out a detailed benchmark of X-ray and EUV Fe XVII lines only, or Liang & Zhao (2010) who used *Chandra*/LETGS Procyon spectra for a comparison of their Fe VII-Fe XVI atomic data with observed spectral lines in the 49-106Å range.

The aim of the present series of papers is to test the CHIANTI atomic data in the 10-170Å wavelength range, which is relevant to *SDO* (AIA and EVE) observations. In this paper, the first of the series, we focus on issues in the wavelength ranges of the two shortest-wavelength AIA channels, centered at 94Å and 131Å. We also provide a broad overview of the shortcomings of CHIANTI in reproducing observed spectra in the 10-170Å, consequential for EVE observations. In the next two papers of the series, we will present a systematic benchmark of the CHIANTI data with the observed lines, ion by ion (Drake et al. 2011 and Landi et al. 2011, in preparation).

Despite the observational attention given to the 10-170 Å wavelength range, in the context of atomic physics it has been somewhat neglected in the recent literature. For the last two decades or so, the atomic data effort stemming from solar physics has been directed toward the wavelength ranges covered by the high-resolution spectrometers on board the Solar and Heliospheric Observatory (*SoHO*) and *Hinode*, all exceeding 170 Å. Also, few high resolution spectra have ever been recorded from the Sun in this range, all of them 25 or more years ago, since most of the rocket- and satellite-borne instrumentation built in the past was optimized to work either

TABLE 1
SUMMARY OF *Chandra* LETG+HRC-S OBSERVATIONS OF PROCYON USED FOR THE ANALYSIS.

Obs. ID	Start (UT)	exp. [ks]	F_X^a [erg cm ² s ⁻¹]	L_X^b [erg s ⁻¹]
63	1999-11-06 21:11:32	69.7	1.95×10^{-11}	3.03×10^{28}
1461	1999-11-07 16:59:48	69.8	1.98×10^{-11}	3.06×10^{28}
10994	2009-12-15 22:05:38	71.3	2.02×10^{-11}	3.15×10^{28}
12042	2009-12-26 01:23:39	65.1	2.01×10^{-11}	3.13×10^{28}

^a X-ray flux in the range 5-165Å ($\approx 0.075 - 2.5$ keV).

^b X-ray luminosity, in the range 5-165Å, corrected for absorption (assuming $N_H = 1.15 \times 10^{18}$ cm⁻²; Linsky et al. 1995).

below 20 Å, or above 170 Å. Ironically, the best spectra in the 10-170 Å wavelength range available today have been observed from much fainter stellar sources with the *Chandra* Low Energy Transmission Grating Spectrometer (LETGS; Brinkman et al. 1987) and, at lower resolution, with the Extreme Ultraviolet Explorer (*EUVE*; Bowyer & Malina 1991). In order to test CHIANTI, we chose to use X-ray/EUV spectra of the low-activity solar-like coronal emission of the subgiant Procyon, observed with *Chandra*/LETGS, which is characterized by spectral resolution ($\Delta\lambda \sim 0.05\text{\AA}$) significantly better than the resolution of EVE ($\Delta\lambda \sim 1\text{\AA}$). Procyon (F5 IV; α CMi, HD 61421; $d=3.51$ pc, van Leeuwen 2007) is one of the brightest stars in the sky and also thanks to its proximity has been very well studied at optical to X-ray energies (e.g., Steffen 1985; Drake et al. 1995; Allende Prieto et al. 2002). The coronal emission of Procyon has been studied in detail in the past three decades at EUV and X-ray wavelength with several instruments (e.g., Lemen et al. 1989; Drake et al. 1995; Raassen et al. 2002), indicating that the X-ray emission is rather constant ($L_X \sim 2 \times 10^{28}$ erg s⁻¹, in the energy range 0.1-2.4 keV based on the *ROSAT* All-Sky Survey; Hünsch et al. 1999), and characterized by a relatively cool plasma thermal distribution that peaks around 1-3 MK. These temperatures are close to values typical of non-flaring solar plasmas, therefore making Procyon an excellent X-ray source to benchmark the atomic data for plasma conditions typically observed by *SDO*.

The observations are described in Section 2. The data analysis and results of the determination of the plasma temperature distribution are presented and discussed in Section 3. We summarize our findings and draw our conclusions in Section 4.

2. OBSERVATIONS AND DATA REDUCTION

We analysed *Chandra* spectra of Procyon obtained in four different pointings (two in November 1999 and two in December 2009), using the LETG and High Resolution Camera spectroscopic detector (HRC-S) in its standard instrument configuration. Observational data were obtained from the public *Chandra* Data Archive, and reduced using the CIAO software package (v4.3). For the analysis presented in this paper, we used the Package for Interactive Analysis of Line Emission (PINTofALE, Kashyap & Drake 2000).

The details of the four *Chandra* observations are listed in Table 1. Light curves derived from the 0th order photon events, binned at an interval of 1ks, are illustrated in

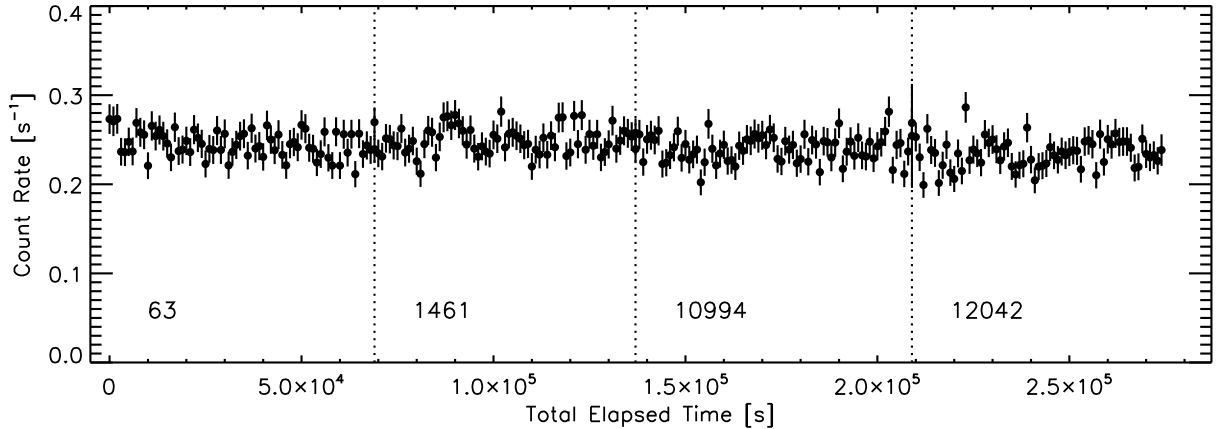


FIG. 1.— Light curves derived for each pointing from the 0th order photon events, binned at an interval of 1ks.

Figure 1 and the spectra extracted from each epoch are shown in Figure 2. Both light curves and spectra show the X-ray emission of Procyon to be remarkably constant, both in terms of flux level and spectral characteristics, and on all observed time scales, from 1ks to much longer timescales of over 10 years. Close inspection of the spectra does reveal some differences, especially between 49 and 69Å, and above 160Å. These can be ascribed to the different effective areas at those wavelengths, due to the wavelengths in the spectra at which the HRC-S plate gaps occur. These vary from epoch to epoch because of the secular aim point drift of *Chandra* relative to the detector coordinate system. We found no evidence for any significant differences between the spectra taken at different epochs outside of the wavelength regions affected by plate gaps. This lack of variability over timescales ranging from ~ 1 ks to about 10 years is remarkable for the X-ray emission of late-type stars. Although the sampling is sparse, this constancy hints at a lack of a large amplitude magnetic activity cycle analogous to that observed for the Sun and seen in X-rays in other low and moderately active stars (e.g., Hempelmann et al. 2006; Favata et al. 2008; Ayres 2009).

3. ANALYSIS METHODS AND RESULTS

In order to assess completeness and accuracy of the CHIANTI atomic database we proceeded as follows: (1) we selected a set of lines formed over a wide temperature range, unblended, and with reliable atomic data; (2) we reconstructed the emission measure distribution, $EM(T)$, of the emitting coronal plasma using the measured fluxes, and finally (3) we synthesized the model spectrum using CHIANTI and the $EM(T)$ derived from the data and compared it with the observed spectrum at all wavelengths.

The line fluxes used for determining the thermal distribution of the plasma are listed in Table 2. The selected lines are formed over a broad temperature range, as indicated by their temperature of maximum formation, covering roughly the interval from $\log(T[K]) \sim 5.7$ to $\log(T[K]) \sim 6.9$ (see Table 2).

We determined the emission measure distribution by using an iterative method based on a Markov-chain Monte Carlo (MCMC) algorithm (see Kashyap & Drake

1998 for details on assumptions and approximations, and also Testa et al. 2011 for further description of the characteristics of the method). The emission measure distribution is reconstructed using the line emissivities from CHIANTI v.6.0.1 (Dere et al. 1997, 2009), and assuming the ionization balance of Bryans et al. (2009).

Previous analyses of X-ray and EUV spectra of Procyon have indicated that the element abundances of its coronal plasma are close to its photospheric abundances (e.g., Drake et al. 1995; Raassen et al. 2002; Sanz-Forcada et al. 2004), which in turn are similar to solar photospheric abundances (e.g., Steffen 1985; Drake & Laming 1995; Bruntt et al. 2010). By using an abundance diagnostic technique based on temperature insensitive line ratios (Drake & Testa 2005; Huenemoerder et al. 2009) we derive an estimate of the Ne/O abundance ratio of $1.3\times$ the solar photospheric value of Grevesse & Sauval (1998). This diagnostic technique uses the measured fluxes of the strong H-like and He-like transitions, lying at the short wavelength range of the *Chandra* spectra. Procyon is characterized by a rather inactive and cool corona, compared with the more active stellar coronae usually observed with *Chandra*. Therefore, even with the long accumulated exposure time of the spectra analyzed here (~ 275 ks) the H-like and He-like lines of the higher Z elements (mainly Mg, Si, S, Fe), which are formed at temperatures higher than the corresponding transitions of Ne and O, are not detected.

We ran the procedure to derive the emission measure distribution several times and ‘manually’ adjusted the abundances of those elements if the agreement with the model was unsatisfactory and the predicted line fluxes for a given element were consistently lower or higher than the observed fluxes. The model we deemed to be best is characterized by photospheric abundances (Grevesse & Sauval 1998), except for N and Ne which are enhanced by 30% and Mg, Ca, and Fe that are enhanced by 50%. While perhaps slightly higher than current assessments of solar-like photospheric abundances in Procyon, our values are not significantly different considering the combined systematic and random errors of photospheric and coronal analyses. We express our derived abundances relative to the reference set of abundances of Grevesse & Sauval (1998), but the choice of reference

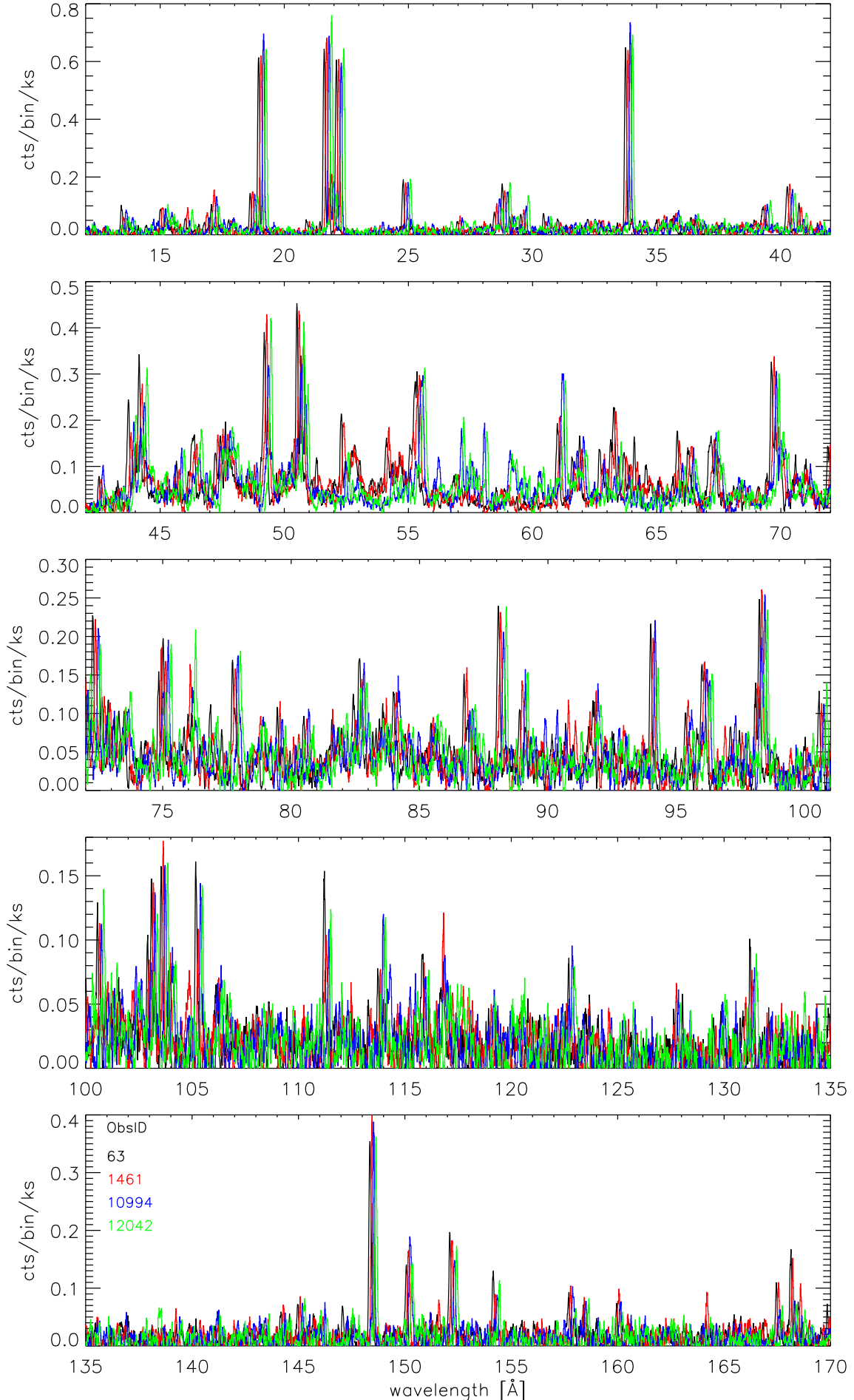


FIG. 2.— Comparison of *Chandra* LETGS spectra of Procyon obtained in four different observations (a different color is used for each observation, as labeled in the bottom plot). For easier comparison each spectrum is shifted by +0.1 Å with respect to the preceding one.

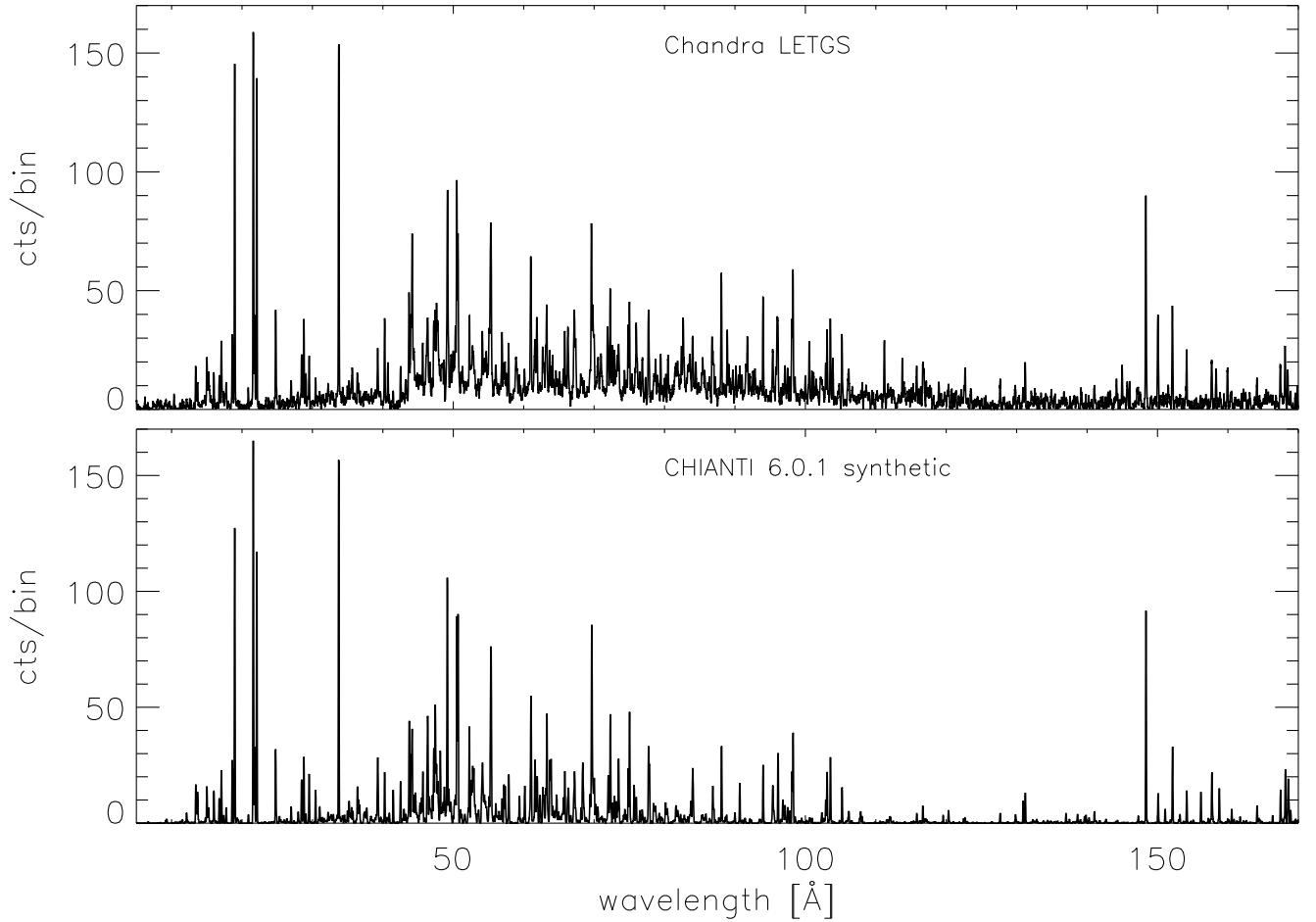


FIG. 3.— *Top*: *Chandra* LETGS spectrum of Procyon, obtained with a total exposure time of approximately 275 ks (Observation ID: 63, 1461, 10994, 12042). *Bottom*: Model spectrum synthesized using CHIANTI 6.0.1 and the emission measure distribution derived from the measured line fluxes listed in Table 2, and plotted in Figure 4. An expanded version of the model and observed spectra, allowing a more detailed comparison, is presented in Figure 5.

is arbitrary. We adopted the set of Grevesse & Sauval (1998) for easier comparison with other works in the literature.

The emission measure distribution derived from the measured fluxes is illustrated in Figure 4. It is a rather smooth and broad function of temperature, with most material found around $\log(T[K]) \sim 6.1 - 6.3$, i.e. at temperatures typical of non-flaring solar coronal plasmas. This emission measure distribution we derive from the long *Chandra*-LETGS exposure compares well with those derived for the same source by Drake et al. (1995) from *EUVE* observations, and by Raassen et al. (2002) from the first two LETGS observations and *XMM-Newton* spectra, having a similar peak temperature (~ 1.5 MK), emission measure value ($\sim 10^{50} \text{ cm}^{-3}$), and width of the distribution. Some small differences are present either side of the EM distribution peak at temperatures of $\log T = 6.0 - 6.4$. Such differences might be expected based on the different global model fitting approach adopted by Raassen et al., in addition to the more up-to-date ionization balance and collisional excitation data used in the current study. In order to evaluate how well the EM(T) of Figure 4 reproduces the observed emission, the measured fluxes are compared with the fluxes

predicted by the model EM(T) in Table 2. Agreement is satisfactory and typically within $\sim 30\%$, which is in accordance with the assessment by Drake et al. (1995) of typical atomic data uncertainties.

In Figure 3 (bottom panel) we show the model spectrum synthesized from the EM(T) of Figure 4 using the CHIANTI database (v.6.0.1) and the element abundances and ionization equilibrium described above. In order to allow a more detailed comparison of the model with the observed spectrum, in Figure 5 we show the two spectra superimposed (observed spectrum in black and model in red).

Figure 3 and 5 demonstrate quite a favorable comparison at the shorter wavelengths. At longer wavelengths, especially in the $\sim 80 - 110 \text{ \AA}$ range, it is apparent that the observed spectrum contains a large number of lines, strong and weak, missing in the CHIANTI spectral model. This missing flux was first noted in earlier work on *EUVE* stellar spectra, including that of Procyon (see, e.g., discussions by Drake 1996; Drake & Kashyap 2001) and was also touched upon by Raassen et al. (2002) in their analysis of the first two LETGS Procyon observations. We also note that analyses of *SDO*-EVE spectra appear to show the same effect: spectral models are

TABLE 2
IDENTIFICATION AND MEASURED FLUXES FROM *Chandra* LETGS
SPECTRAL OBSERVATIONS OF PROCYON (~ 275 KS).

λ [Å]	Ion	$\log(T_{\max}[\text{K}])$	flux [10^{-6} ph cm $^{-2}$ s $^{-1}$]	$\text{flux}_{\text{pred}}/\text{flux}_{\text{obs}}$
12.1324	Ne x	6.75	$5.82^u \pm 1.8$	0.56
13.4417	Ne ix	6.60	18.6 ± 1.8	1.2
13.6852	Ne ix	6.60	14.4 ± 1.4	1.2
15.0070	Fe xvii	6.80	24.2 ± 1.8	1.1
15.9958	O viii	6.50	17.6 ± 1.8	1.2
16.0590	Fe xviii	6.90	$2.15^u \pm 1.3$	0.62
16.7783	Fe xvii	6.70	16.0 ± 1.5	1.2
17.0768	Fe xvii	6.70	53.6 ± 2.9	0.82
18.6271	O vii	6.30	46.7 ± 2.8	0.85
18.9651	O viii	6.50	224 ± 10	0.95
21.6077	O vii	6.30	379 ± 15	1.1
21.8064	O vii	6.30	95.0 ± 4.9	1.0
22.0979	O vii	6.30	335 ± 11	0.87
24.7879	N vii	6.30	102 ± 6.2	0.84
28.4630	C vi	6.15	55.9 ± 4.0	0.87
28.7769	N vi	6.15	91.5 ± 5.1	0.86
29.0736	N vi	6.10	30.9 ± 3.0	0.83
29.5386	N vi	6.10	51.7 ± 4.1	0.96
30.4453	Ca xi	6.30	34.5 ± 3.7	1.3
33.7451	C vi	6.10	508 ± 19	1.1
34.9869	C v	6.00	23.2 ± 2.9	0.86
39.2737	S xi	6.30	69.5 ± 5.8	0.75
40.7251	C v	5.95	190 ± 16	0.55
43.7323	Si xi	6.30	68.4 ± 3.5	0.90
43.9891	Si xii	6.30	42.2 ± 3.1	0.81
44.1380	Si xii	6.30	61.6 ± 3.7	1.1
45.4889	Si xii	6.30	18.8 ± 1.9	0.96
45.6569	Si xii	6.30	40.6 ± 2.7	0.91
46.3715	Si ix	6.20	31.9 ± 2.7	1.5
47.2280	Si ix	6.10	32.7 ± 2.9	1.3
47.6279	Si x	6.20	48.0 ± 3.7	1.0
47.7801	S x	6.20	25.4 ± 2.7	0.78
49.1922	Si xi	6.25	125 ± 10	1.1
50.5078	Si x	6.20	166 ± 10	0.77
61.0172	Si viii	6.00	154 ± 11	0.57
63.1306	Si x	6.10	70.1 ± 6.6	0.96
63.2662	Si x	6.10	126 ± 12	0.95
65.6395	Si x	6.10	41.9 ± 4.1	0.87
65.8299	Si x	6.10	67.0 ± 5.0	1.1
67.2169	Si ix	6.00	57.0 ± 5.0	1.0
71.9973	S vii	5.80	51.9 ± 4.6	1.0
72.2828	Mg ix	6.00	134 ± 9.7	1.1
72.8687	S vii	5.80	43.4 ± 4.5	0.86
77.7143	Mg ix	6.00	106 ± 7.0	1.1
88.0453	Ne viii	5.85	173 ± 10	0.71
96.0970	Fe x	6.10	139 ± 10.4	0.94
97.4721	Ne vii	5.80	62.3 ± 6.7	0.68
98.0717	Ne viii	5.80	145 ± 10	0.89
98.2259	Ne viii	5.80	238 ± 16	1.1
97.1081	Fe x	6.10	58.6 ± 6.9	0.61
102.898	Ne viii	5.80	84.3 ± 8.1	0.85
103.087	Ne viii	5.80	137 ± 10	1.1
103.547	Fe ix	5.90	208 ± 13	0.78
105.183	Fe ix	5.90	157 ± 11	0.59
127.649	Ne vii	5.75	113 ± 12	0.65
130.940	Fe viii	5.70	69.5 ± 12	1.4
131.227	Fe viii	5.70	172 ± 15	1.1
148.358	Ni xi	6.10	908 ± 37	1.2
152.117	Ni xii	6.20	420 ± 26	0.86
154.143	Ni xii	6.20	276 ± 21	0.67
157.684	Ni xiii	6.30	156 ± 18	1.7
167.459	Fe viii	5.70	659 ± 59	1.1
168.130	Fe viii	5.70	971 ± 72	1.2
168.497	Fe viii	5.70	583 ± 57	1.0
168.895	Fe viii	5.70	317 ± 44	0.98

^u The label “u” associated with a flux value indicates an upper limit.

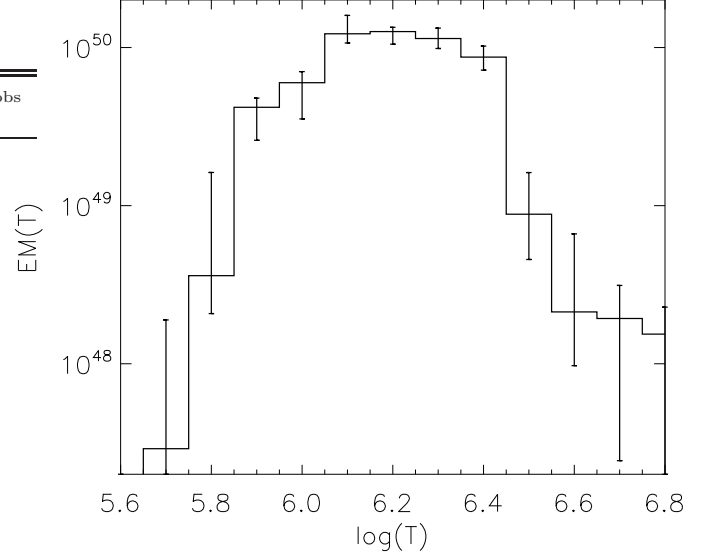


FIG. 4.— Emission measure distribution, $\text{EM}(T)$, derived applying a Markov Chain Monte Carlo (MCMC) iterative method to the measured fluxes of the lines listed in Table 2.

in good agreement with the observed spectra at EUV wavelengths ($\gtrsim 150\text{\AA}$) whereas they represent a poor match to the observed emission in the $\sim 50 - 150\text{\AA}$ range (H. Warren, private communication). These findings strongly suggest that the missing flux is not due to inadequate modeling of transitions included in current databases but to incompleteness atomic databases at those wavelengths. In order to estimate the effect of the flux apparently lacking in the model spectrum on the analysis of EVE spectra, we degraded both the model and the observed spectrum to EVE spectral resolution and plot their ratio in Figure 6. This plot shows that the model underestimates the observed flux by a variable factor ranging from ≈ 1.5 , at short wavelengths below $\sim 50\text{\AA}$, up to $\approx 5-7$ in the $\sim 70 - 125\text{\AA}$ range. We defer a more detailed discussion to Drake et al. (2011, in preparation).

Figure 7 shows the comparison of the spectral model and observations in the wavelength ranges of the AIA passbands centered on 94\AA and 131\AA (171\AA is at the edge of the sensitivity of *Chandra*-LETGS). These plots demonstrate that the model lacks a significant portion of the observed flux, especially in the 94\AA range. In particular, in the 94\AA band, not only is the strongest feature, Fe xviii $93.93\text{\AA} + \text{Fe x } 94.01\text{\AA}$, significantly underestimated by the model, but the observed level of emission is consistently higher than the model throughout the bandpass. This is likely due to the contribution of a large number of relatively weak lines that form a pseudo-continuum which becomes comparable in flux to the resolved lines. In the 131\AA band, the disagreement is less severe: the predicted fluxes of the strong Fe viii lines are close to the measured values, though the flux contribution of weaker lines is underpredicted (or completely lacking) in the model. We note that neither the uncertainties on the background subtraction nor the possible contamination from the overlapping higher spectral orders can explain the observed discrepancies (in Figure 7

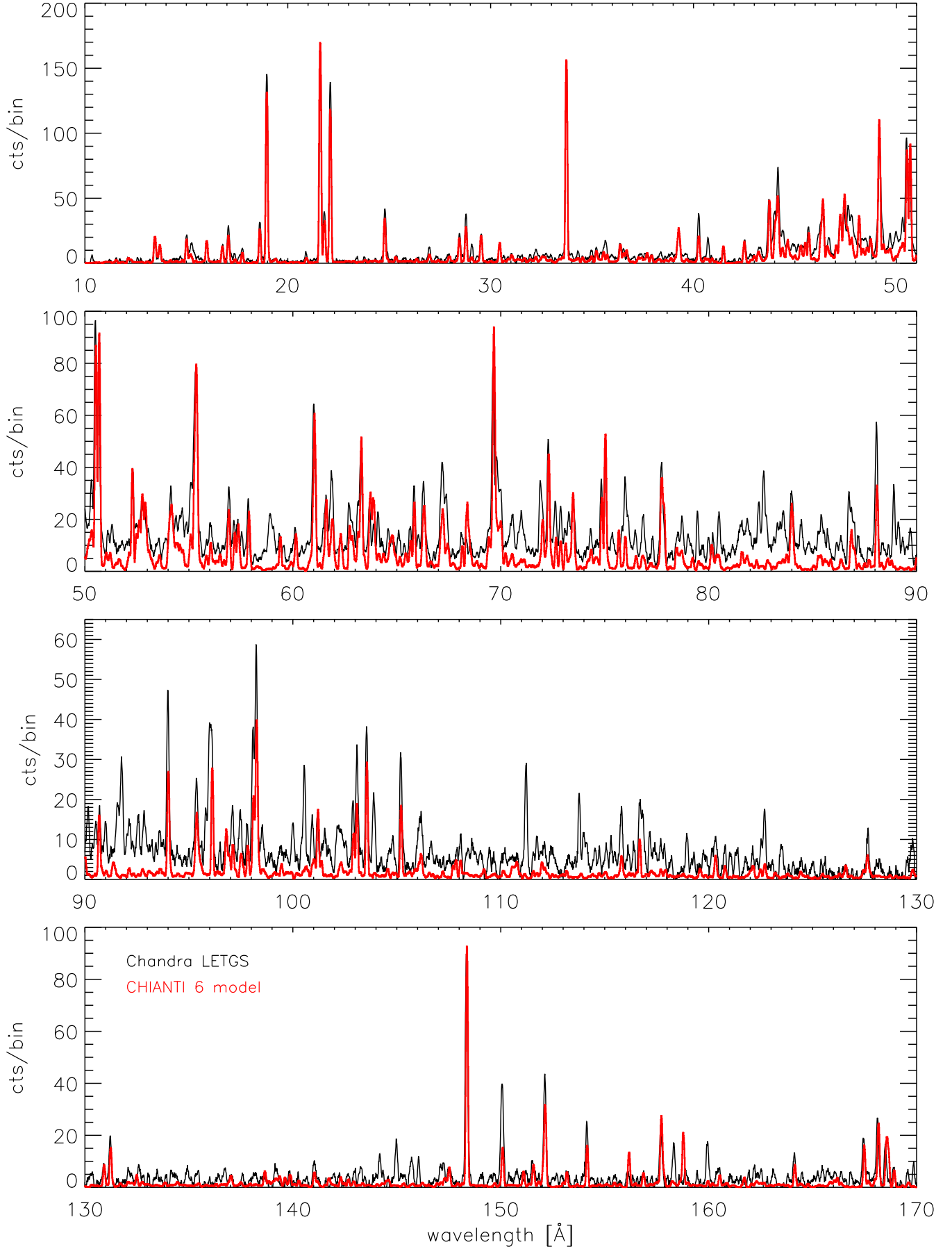


FIG. 5.— Comparison of *Chandra* LETGS observations (black) and CHIANTI 6 model (red; including orders $\pm 1,2,3$) synthesized using the EM(T) shown in Figure 4, derived using the line fluxes of Table 2.

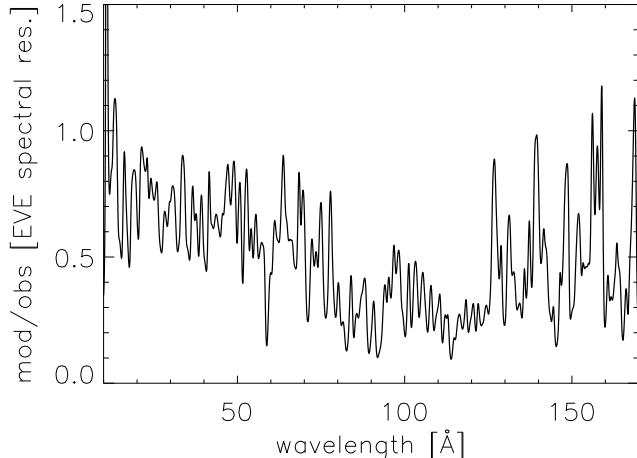


FIG. 6.— Ratio of the CHIANTI model spectrum to the observed spectrum, both degraded to the EVE spectral resolution.

we also show separately the modeled high order contribution, as a blue dotted curve).

In order to estimate what the effect of the missing flux would be on an AIA observation of coronal plasma with Procyon-like X-ray-EUV emission, we convolved the observed and modeled spectrum with the responses of the AIA 94Å and 131Å narrow passbands as a function of wavelength. We find that the AIA flux for a Procyon-like source would be underestimated by the spectral model by a factor of roughly 3 in the 94Å passband and 1.9 in the 131Å passband. The plots of the observed and model spectra folded with the AIA responses in the 94Å and 131Å channels (bottom panels of Figure 7), clearly show which spectral features are more relevant, contributing more significantly to the AIA intensity.

Laboratory experiments with the Lawrence Livermore electron beam ion trap, EBIT, (Beiersdorfer et al. 1999; Lepson et al. 2002) focusing on the wavelength range $\approx 60 - 140$ Å investigated the presence of Fe lines (Fe VII–X) possibly not included in current atomic databases and potentially important for the interpretation and modeling of solar and stellar soft X-ray-EUV spectra. We reviewed their findings to explore whether any of their detected emission lines that are still absent from atomic databases might affect significantly the 94Å and 131Å AIA wavelength ranges. In their list of emission lines, we find that there are two transitions with potentially significant impact for the 94Å AIA passband. These are two Fe IX lines – $3p^5 5f \rightarrow 3p^5 3d$ transitions – with measured wavelengths of λ 93.59Å and 94.07Å respectively (Lepson et al. 2002), and intensities of roughly 0.25 and $0.3\times$ the intensity of the Fe IX emission at 103.55Å. We note that the intensities reported in these laboratory experiments cannot be directly translated into relative intensity expected for the emission of coronal plasma, as in EBIT experiments the plasma conditions can significantly deviate from the conditions generally assumed for coronal thermal plasma (for instance the electrons have non-Maxwellian distribution). Foster & Testa (2011) used the Flexible Atomic Code to carry out calculations for these Fe IX transitions, and we explore the

possible relevance of these lines to explain the missing flux, by recomputing the model adding these additional Fe IX contributions in the 94Å range to the synthetic CHIANTI model spectrum. This new spectral model including the Fe IX transitions, shown in Figure 8 (blue line), is in much better agreement with the observed spectrum in that narrow wavelength range, and reduces the flux discrepancy from the factor ~ 3 for the pure CHIANTI 6 spectrum to roughly 80%.

If we include the contribution functions of these Fe IX lines, we can estimate the impact on the temperature response of the AIA 94Å passband. The “corrected” AIA temperature response is shown in Figure 9, compared to the default response computed using CHIANTI 6. Addition of the Fe IX contribution increases the response of the AIA 94Å channel by roughly a factor 2 in the cool temperature range (see also Foster & Testa 2011, where APED is used; Smith et al. 2001).

In the 131Å wavelength region, none of the lines identified in Lepson et al. (2002) appear to have significant impact for AIA observations. However, some might be relevant to the analysis of EVE spectra, such as for instance two Fe IX $3p^5 4f \rightarrow 3p^5 3d$ transitions with measured wavelengths of λ 134.08Å and 136.70Å (see discussion in Foster & Testa 2011, where a synthetic spectrum including these transitions is compared with a EVE quiet Sun spectrum). Besides these lines around ~ 94 Å and ~ 135 Å, the new calculations presented in Foster & Testa 2011 indicate that the added Fe IX transitions provide only limited additional flux in the 10–170Å band, compared to current versions of atomic databases. This modest additional emission is expected around 82Å, in the 110–115Å range, and around ~ 164 Å where the model predicts a strong 4p–3d transition.

The study by Liang & Zhao (2010) is also potentially helpful for identifying lines missing in the atomic databases. They compare their Fe VII–Fe XVI atomic data with *Chandra*/LETGS observations of Procyon. As they note, CHIANTI 6 only includes data from $n=3$ levels for Fe IX, Fe XII, Fe XIII, Fe XIV, and the missing lines from these ions might contribute non-negligible flux in the 10–170Å wavelength range. Although we use a set of spectral observations partially overlapping with those used by Liang & Zhao (2010), their aim and methods were different with respect to ours. They carry out a detailed comparison of their theoretical models with existing alternative atomic data focusing exclusively on Fe VII–Fe XVI lines, and they did not analyze the spectra longward of 106Å. Also, they used a simplified 3 temperature model from Raassen et al. (2002) which is expected to be a less accurate representation of the temperature distribution of the coronal plasma compared to the emission measure distribution we use here and therefore lead to a less accurate reproduction of the line fluxes in the whole wavelength range (see also above comparison of our finding for the EM(T) with the results of Raassen et al. 2002). Finally, the total exposure time of the observations we analyze here is almost twice as long as the one used by Liang & Zhao (2010), improving the signal-to-noise ratio of the spectrum. For the 94Å wavelength range, they noted problems in their model for Fe X, which is predicting the 94.02Å flux to be much lower than the CHIANTI

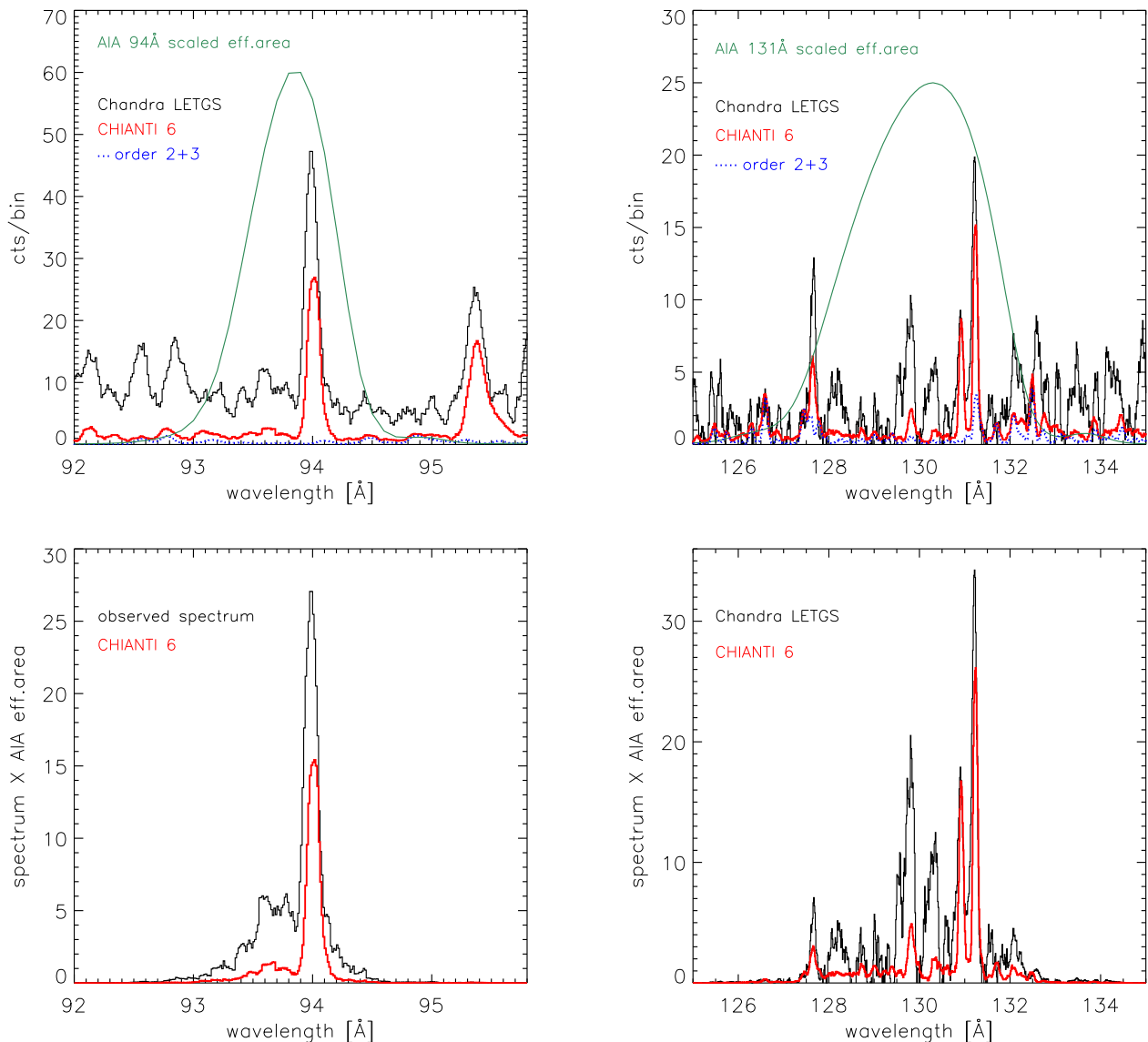


FIG. 7.— *Top*: observed LETGS spectrum of Procyon (black curve) and model (total of orders 1, 2, and 3, positive and negative; red curve) in the wavelength regions observed by the shortest wavelength narrow-bands of the Atmospheric Imaging Assembly (AIA) on the Solar Dynamics Observatory. Scaled effective areas for the 94Å, and 131Å, AIA passbands (green curves) are superimposed to indicate the sensitivity of AIA to the spectral features in each wavelength range. We also plot the high order ($\pm 2, 3$) contribution to the spectrum model. *Bottom*: Observed and model spectrum (black and red respectively) multiplied by the AIA effective area in the 94Å channel (*left*) and 131Å channel (*right*). These curves show the contribution of the different spectral features to the AIA observed intensity.

6 expected flux (and much lower than the observed flux). They did not include the Fe IX lines around $\sim 94\text{\AA}$ observed in the EBIT experiments (Lepson et al. 2002).

We note that recent analyses of AIA data have highlighted issues with the observed fluxes in the 94Å and 131Å passbands, suggesting that (cool) lines missing in the atomic databases are the likely cause (Schmelz et al. 2011; Aschwanden & Boerner 2011). Aschwanden & Boerner (2011) also attempted an estimate of the correction factor for the response of the 94Å AIA channel to the cool (1MK) plasma, by analyzing a sample of loops for which emission in the other AIA bands is compatible with a near isothermal emission measure distribution. They derive a factor of 6.7 ± 1.7 , which

is significantly larger than the contribution of Fe IX estimated by Foster & Testa (2011) and in this work, suggesting that other ions also provide non-negligible contributions³.

In the 131Å range the EBIT experiments suggest the presence of several Fe VII lines, in the 127-134Å range, which are not included in CHIANTI 6.0.1 (or APED) and might provide significant contribution. Also a Fe IX line (134.08Å) and a Fe X line (134.09Å) are observed in the EBIT spectra, though their contribution might be rather limited given that the AIA response at those wave-

³ Boerner et al. (in preparation) by looking at the morphology of quiet Sun in deep exposures in the AIA passbands suggest possible additional contribution of emission from $\log T[K] \sim 6.0 - 6.3$.

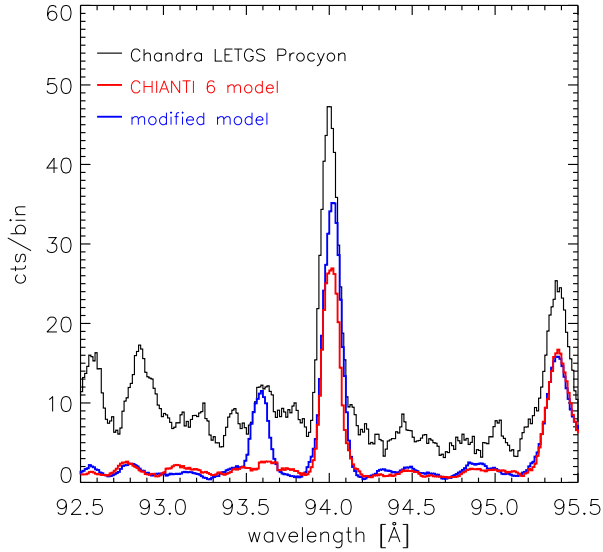


FIG. 8.— A modified spectral model (blue), with the addition of an empirical correction to the CHIANTI model including Fe IX transitions observed in laboratory experiments (see text and Foster & Testa 2011) and not present in the CHIANTI atomic database, is superimposed to the CHIANTI 6 model (red) and observed spectra (black).

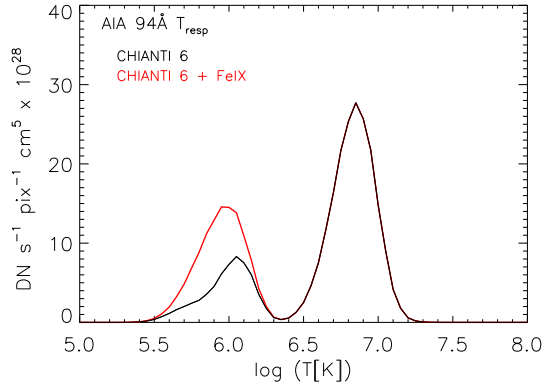


FIG. 9.— Temperature response of AIA in the 94 Å passband: the black line represents the default response, obtained using the CHIANTI database (v.6.0.1), ionization equilibrium by Bryans et al. (2009) and solar coronal abundances (Feldman 1992); the red curve represents the response including the contribution of Fe IX lines (Foster & Testa, 2011) not included in CHIANTI but observed in laboratory experiments (Lepson et al. 2002).

lengths is already roughly two orders of magnitudes lower than at its peak. Additional contribution can also come from ions other than the Fe VII–Fe X studied in the EBIT laboratory experiments. In particular L-shell transitions of Mg and Ne are expected to fall around 94 Å and 132 Å. At the time of writing, the new version of the CHIANTI database (v7) is still under testing, though based on the changes in the ions relevant to the AIA bandpasses under consideration no significant differences are expected.

4. CONCLUSIONS

High-resolution X-ray spectra of the low-activity solar-like corona of Procyon obtained with the *Chandra* Low Energy Transmission Grating Spectrometer (LETGS) have been used for testing the X-ray/EUV data in the CHIANTI database. A systematic benchmark ion by ion will be presented in two future papers (Drake et al. 2011, and Landi et al., 2011, in preparation). Model and observed spectra are in reasonably good agreement in the soft X-ray range ($\lambda \lesssim 50$ Å) and at the longer LETGS wavelengths $\lambda \gtrsim 130$ Å. However, the model flux lies significantly below the observed flux in the 50–130 Å wavelength range. In particular, in the 94 Å and 131 Å AIA bands the observed flux exceeds the model flux by factors of ~ 3 and ~ 1.9 , respectively. By including two relatively strong Fe IX lines at λ 93.59 Å and 94.07 Å observed in the laboratory by Lepson et al. (2002), the discrepancy in the 94 Å band is reduced to $\sim 80\%$. The AIA temperature response corrected in this way is increased by roughly a factor of 2 at 10^6 K. In the 131 Å band, Fe VII transitions, not included in CHIANTI but observed in laboratory experiments, as well as L-shell Ne transitions, might explain part of the missing flux.

We thank Adam Foster for useful discussion, and the referee for comments that have helped improve the paper. PT was supported by contract SP02H1701R from Lockheed-Martin to the Smithsonian Astrophysical Observatory. JJD was supported by NASA contract NAS8-39073 to the *Chandra* X-ray Center and thanks the Director, H. Tananbaum, for continuing support. The work of EL is supported by the NNX11AC20G and NNX10AM17G grants to the University of Michigan, and grant SV1-81002 to the Smithsonian Astrophysical Observatory.

REFERENCES

- Allende Prieto, C., Asplund, M., García López, R. J., & Lambert, D. L. 2002, *ApJ*, 567, 544
 Anders, E., & Grevesse, N. 1989, *Geochim. Cosmochim. Acta*, 53, 197
 Aschwanden, M. J., & Boerner, P. 2011, *ApJ*, 732, 81
 Ayres, T. R. 2009, *ApJ*, 696, 1931
 Beiersdorfer, P., Lepson, J. K., Brown, G. V., Utter, S. B., Kahn, S. M., Liedahl, D. A., & Mauche, C. W. 1999, *ApJ*, 519, L185
 Boerner, P., et al. 2011, *Sol. Phys.*, submitted
 Bowyer, S., & Malina, R. F. 1991, *Advances in Space Research*, 11, 205
 Brinkman, A. C., van Rooijen, J. J., Bleeker, J. A. M., Dijkstra, J. H., Heise, J., de Korte, P. A. J., Mewe, R., & Paerels, F. 1987, *Astrophysical Letters Communications*, 26, 73
 Bruntt, H., et al. 2010, *MNRAS*, 405, 1907
 Bryans, P., Landi, E., & Savin, D. W. 2009, *ApJ*, 691, 1540
 Dere, K. P., Landi, E., Mason, H. E., Monsignori Fossi, B. C., & Young, P. R. 1997, *A&AS*, 125, 149
 Dere, K. P., Landi, E., Young, P. R., Del Zanna, G., Landini, M., & Mason, H. E. 2009, *A&A*, 498, 915
 Del Zanna, G., & Ishikawa, Y. 2009, *A&A*, 508, 1517
 Drake, J. J. 1996, in *Astronomical Society of the Pacific Conference Series*, Vol. 109, *Cool Stars, Stellar Systems, and the Sun*, ed. R. Pallavicini & A. K. Dupree, 203–+
 Drake, J. J., & Kashyap, V. 2001, *ApJ*, 547, 428
 Drake, J. J., & Laming, J. M. 1995, *The Observatory*, 115, 118
 Drake, J. J., Laming, J. M., & Widing, K. G. 1995, *ApJ*, 443, 393
 Drake, J. J., & Testa, P. 2005, *Nature*, 436, 525
 Favata, F., Micela, G., Orlando, S., Schmitt, J. H. M. M., & Sciortino, S. 2008, *A&A*, 490, 1121
 Feldman, U. 1992, *Phys. Scr*, 46, 202

- Foster, A., Smith, R. K., Brickhouse, N. S., & Kallman, T. R. 2010, in *Bulletin of the American Astronomical Society*, Vol. 42, AAS/High Energy Astrophysics Division #11, 678—
- Foster, A., & Testa, P. 2011, *ApJ*, submitted
- Grevesse, N., & Sauval, A. J. 1998, *Space Science Reviews*, 85, 161
- Hempelmann, A., Robrade, J., Schmitt, J.H.M.M., Favata, F., Baliunas, S. L., & Hall, J. C. 2006, *A&A*, 460, 261
- Huenemoerder, D. P., Schulz, N. S., Testa, P., Kesich, A., & Canizares, C. R. 2009, *ApJ*, 707, 942
- Hünsch, M., Schmitt, J. H. M. M., Sterzik, M. F., & Voges, W. 1999, *A&AS*, 135, 319
- Kashyap, V., & Drake, J. J. 1998, *ApJ*, 503, 450
- . 2000, *Bulletin of the Astronomical Society of India*, 28, 475
- Landi, E., Feldman, U., & Dere, K. P. 2002a, *ApJ*, 574, 495
- . 2002b, *ApJS*, 139, 281
- Landi, E., & Phillips, K. J. H. 2006, *ApJS*, 166, 421
- Lemen, J., Title, A., Akin, D., Boerner, P., Chou, C., & et al. 2011, *Sol. Phys.*, submitted
- Lemen, J. R., Mewe, R., Schrijver, C. J., & Fludra, A. 1989, *ApJ*, 341, 474
- Lepson, J. K., Beiersdorfer, P., Brown, G. V., Liedahl, D. A., Utter, S. B., Brickhouse, N. S., Dupree, A. K., Kaastra, J. S., Mewe, R., & Kahn, S. M. 2002, *ApJ*, 578, 648
- Liang, G. Y., & Zhao, G. 2010, *MNRAS*, 405, 1987
- Linsky, J. L., Diplas, A., Wood, B. E., Brown, A., Ayres, T. R., & Savage, B. D. 1995, *ApJ*, 451, 335
- Pawlowski, D. J., & Ridley, A. J. 2008, *Journal of Geophysical Research (Space Physics)*, 113, 10309
- Phillips, K. J. H., Mewe, R., Harra-Murnion, L. K., Kaastra, J. S., Beiersdorfer, P., Brown, G. V., & Liedahl, D. A. 1999, *A&AS*, 138, 381
- Raassen, A. J. J., Mewe, R., Audard, M., Güdel, M., Behar, E., Kaastra, J. S., van der Meer, R. L. J., Foley, C. R., & Ness, J.-U. 2002, *A&A*, 389, 228
- Sanz-Forcada, J., Favata, F., & Micela, G. 2004, *A&A*, 416, 281
- Schmelz, J. T., Jenkins, B. S., Worley, B. T., Anderson, D. J., Pathak, S., & Kimble, J. A. 2011, *ApJ*, 731, 49
- Smith, R. K., Brickhouse, N. S., Liedahl, D. A., & Raymond, J. C. 2001, *ApJ*, 556, L91
- Steffen, M. 1985, *A&AS*, 59, 403
- Testa, P., Reale, F., Landi, E., DeLuca, E. E., & Kashyap, V. 2011, *ApJ*, 728, 30
- van Leeuwen, F. 2007, *A&A*, 474, 653
- Woods, T. N., et al. 2004, *Geophys. Res. Lett.*, 31, L10802
- Woods, T. N., et al. 2010, *Sol. Phys.*, 3
- Young, P. R., Landi, E., & Thomas, R. J. 1998, *A&A*, 329, 291